JOURNAL OF COMPUTATIONAL PHYSICS 30, 181–201 (1979)

# A Finite Element for the Numerical Solution of Viscous Incompressible Flows

MICHEL BERCOVIER AND MICHAEL ENGELMAN

*Hebrew University, Computation Center and Institute of Mathematics and Graduate School of Applied Sciences, Jerusalem, Israel*

Received July 11, 1977; revised January 9, 1978

A finite element of the penalization type for the solution of incompressible viscous Navier–Stokes equations using an isoparametric parabolic element is presented. The penalization of the continuity equation is implemented by means of a reduced integration technique, thus eliminating the pressure unknown from the system of equations to be solved. The superiority of the nine-node isoparametric quadrilateral element over the eight-node element is discussed. Stability and convergence properties of the method are illustrated by means of various numerical examples.

## INTRODUCTION

A finite element of the so-called penalization type, studied in [1], is used to solve several model problems of viscous incompressible flows in $R^2$. Most of the finite element solutions for this class of problems are of the "mixed" type, requiring the use of the pressure term, thus limiting the size of the problems (cf. Taylor and Hood [18]). To overcome this difficulty two approaches have been suggested: the use of saddle point algorithms (see Teman [20]) and the use of penalization and reduced integration (Naylor [16]). Our approach is of the second type, but instead of using an 8-node element which is not always consistent (cf. [1]) we use the 9-node parabolic ($Q_2$) isoparametric element.

In order to deal with the condition "div $\mathbf{u} = 0$" without introducing Lagrange multipliers, a penalization with reduced integration "trick" is used. This technique was first introduced by Zienkiewicz *et al.* [22] for shells and later used in flow problems by Zienkiewicz and Godbole [21]. This enables us to show that the penalization is in fact a regularization of the mixed variational formulation [1], and none of the usual limitations of the penalization method interferes with our approximation. We are then in a position to solve problems with realistic discretizations with computing times that are quite competitive with accepted finite difference schemes.

The use of reduced integration (which is limited to the penalty term only) is actually equivalent to the weakening of the constraint div $\mathbf{u} = 0$. The necessity of such a weakening in mixed finite element techniques is well known and error estimates have also been established (cf. Fortin [8] and Crouzieux and Raviart [7]).



0021-9991/79/020181–21$02.00/0

Copyright © 1979 by Academic Press, Inc.
All rights of reproduction in any form reserved.

The proof of the duality of the two approaches has been given by Malkus [14, 15] in the linear case and independently by Bercovier [1] where the Navier–Stokes equations are also treated. Hughes *et al.* [12] used a bilinear element together with a reduced integration technique to solve incompressible viscous flows; a related four-node element can also be found in Bercovier and Livne [2].

The penalization approach can also be applied without the use of reduced integration. In this event, the accuracy of the results is dependent on the choice of an optimal penalty parameter, which has been shown by Fried [10] to be a function of mesh size. A method of overcoming this problem by the combined use of penalization and extrapolation was given by Falk [9]. Both these studies considered only the linear case but they can be extended to the nonlinear case by use of the results of Pelissier [17].

## 2. Perturbation of the Navier–Stokes Equations

Let $\Omega$ be a bounded domain of $R^2$. Let $\partial\Omega$ be its boundary. We want to compute an approximate solution to the dimensionless problem:

Find $\mathbf{u}$ and $p$ such that

$$\frac{\partial \mathbf{u}}{\partial t} + \mathbf{u} \cdot \nabla \mathbf{u} - \frac{1}{R} \nabla^2 \mathbf{u} + \nabla p = \mathbf{f} \qquad \text{in } \Omega, \tag{1}$$

$$\mathbf{u} = \boldsymbol{\alpha}; \qquad \boldsymbol{\alpha} = \boldsymbol{\alpha}(x, y, t), \qquad \text{on } \partial\Omega, \tag{2}$$

$$\mathbf{u}\,|_{t=0} = \mathbf{u}_0\,; \qquad \mathbf{u}_0 = \mathbf{u}_0(x, y, t) \qquad \text{in } \Omega, \tag{3}$$

where $R$ is the Reynolds number of the flow.

In order to obtain our approximations we first introduce a set of equations with a small perturbation. (Note that we do not have what is called a slightly compressible flow in what follows, but it does belong to the same family of approximations introduced by Chorin [5].)

Consider the following problem:

Find $\mathbf{u}$ such that:

$$\frac{\partial \mathbf{u}_\epsilon}{\partial t} + \mathbf{u}_\epsilon \cdot \nabla \mathbf{u}_\epsilon - \frac{1}{R} \nabla^2 \mathbf{u}_\epsilon + \frac{1}{2} (\operatorname{div} \mathbf{u}_\epsilon)\, \mathbf{u}_\epsilon - \frac{1}{\epsilon} \nabla (\operatorname{div} \mathbf{u}_\epsilon) = \mathbf{f}, \tag{1'}$$

$$\mathbf{u} = \boldsymbol{\alpha} \qquad \text{on } \partial\Omega, \tag{2'}$$

$$\mathbf{u}\,|_{t=0} = \mathbf{u}_0 \qquad \text{in } \Omega, \tag{3'}$$

and the corresponding problem for the steady state case. Introduction of the term $\frac{1}{2}(\operatorname{div} \mathbf{u}_\epsilon)\mathbf{u}_\epsilon$ which defines (1′)–(3′) as a "well-posed" problem is due to Teman [19], who showed that if this term is not present then the system is not a Cauchy–Kowaleski system; in which case uniqueness and convergence for the system is an open question. Here the condition $\operatorname{div} \mathbf{u} = 0$ is replaced by the penalization term $(1/\epsilon)\, \nabla(\operatorname{div} \mathbf{u}_\epsilon)$.

Let $V = (H_0^1(\Omega))^2$, $\tilde{W} = L^2(\Omega)/R$, $W = L^2(\Omega)$. Then in the steady state homogeneous boundary condition case, with appropriate hypotheses on $\Omega$ and $\mathbf{f}$, one can show (cf. [20]) that:

$$\| \mathbf{u} - \mathbf{u}_\epsilon \|_V + \| p - p_\epsilon \|_W \leqslant C\epsilon \tag{5}$$

where $(\mathbf{u}, p)$ is the solution of the original problem and $p = -(1/\epsilon) \cdot \operatorname{div} \mathbf{u}_\epsilon$, and $C$ is a constant depending on $\mathbf{f}$, $\Omega$, $R$ but not on $\epsilon$. $V$ is the product Sobolev space $H_0^1(\Omega) \times H_0^1(\Omega)$ and $W$ is $L^2(\Omega)/R$, both having the standard norms $\| \cdot \|_V$, $\| \cdot \|_W$.

Formulation (1′)–(3′) was studied by Teman [19] for finite difference schemes. The extension to a class of finite element approximations is the aim of this paper.

*Mixed Variational Formulation*

In order to clarify the main points of the analysis we shall consider here only the homogeneous boundary condition steady state case.

Let us define on $V \times V$ a bilinear form:

$$a(\mathbf{u}, \mathbf{v}) = \left(\frac{\partial \mathbf{u}}{\partial x_1}, \frac{\partial \mathbf{v}}{\partial x_1}\right) + \left(\frac{\partial \mathbf{u}}{\partial x_2}, \frac{\partial \mathbf{v}}{\partial x_2}\right)$$

and consider two trilinear forms on $V^3$:

$$b(\mathbf{u}, \mathbf{v}, \mathbf{w}) = \left(u_1 \frac{\partial v_1}{\partial x_1} + u_2 \frac{\partial v_1}{\partial x_2}, w_1\right) + \left(u_1 \frac{\partial v_2}{\partial x_1} + u_2 \frac{\partial v_2}{\partial x_2}, w_2\right),$$

$$\hat{b}(\mathbf{u}, \mathbf{v}, \mathbf{w}) = \tfrac{1}{2}(b(\mathbf{u}, \mathbf{v}, \mathbf{w}) - b(\mathbf{u}, \mathbf{w}, \mathbf{v})).$$

We can now introduce the mixed variational formulation for the Navier–Stokes equations:

*Problem P.* Find $(\mathbf{u}, p) \in V \times \tilde{W}$ such that

$$(1/R)\, a(\mathbf{u}, \mathbf{v}) + \hat{b}(\mathbf{u}, \mathbf{u}, \mathbf{v}) - (\operatorname{div} \mathbf{v}, p) = (\mathbf{f}, v), \tag{6a}$$

$$(\operatorname{div} \mathbf{u}, q) = 0 \tag{6b}$$

for all $\{\mathbf{v}, q\} \in V \times \tilde{W}$.

The corresponding perturbed problem is:

*Problem $P_\epsilon$.* Find $(\mathbf{u}_\epsilon, p_\epsilon) \in V \times W$ such that

$$(1/R)\, a(\mathbf{u}_\epsilon, \mathbf{v}) + \hat{b}(\mathbf{u}_\epsilon, \mathbf{u}_\epsilon, \mathbf{v}) - (\operatorname{div} \mathbf{v}, p_\epsilon) = (\mathbf{f}, \mathbf{v}), \tag{6′a}$$

$$\epsilon(p_\epsilon, q) + (\operatorname{div} \mathbf{u}_\epsilon, q) = 0 \tag{6′b}$$

for all $\{\mathbf{v}, q\} \in V \times W$.

In this report we suppose that the data $\partial\Omega$, $\mathbf{f}$, $\alpha$, and $\mathbf{u}_\epsilon$ are smooth enough so that the weak form of our problem is equivalent to (1), (2), and (3) and that we can have error estimates on parabolic Langrangian interpolation.

Let us introduce:

$$N = \sup \frac{|\hat{b}(\mathbf{u}, \mathbf{v}, \mathbf{w})|}{\|\mathbf{u}\|_V \|\mathbf{v}\|_V \|\mathbf{w}\|_V}, \qquad \mathbf{u}, \mathbf{v}, \mathbf{w} \in V$$

and the following hypothesis:

(H.1) $\mathbf{f}$ is such that $NR^2 \|\mathbf{f}\|_V \leqslant 1 - \delta$, $\delta > 0$.

Let $V_h \in V$ and $W_h \in W$ be two finite-dimensional subspaces, let $\text{div}_h(\cdot, \cdot)$ be a bilinear operator on $V \times W_h$ such that

$$(\text{div}_h \mathbf{u}, p_h) = (\text{div}\, \mathbf{u}, p_h) \qquad \text{for all} \quad \mathbf{u} \in V \quad \text{and} \quad p_h \in W_h. \tag{7}$$

Define

$$N_h = \sup \frac{|\hat{b}(\mathbf{u}_h, \mathbf{v}_h, \mathbf{w}_h)|}{\|\mathbf{u}_h\|_{V_h} \|\mathbf{v}_h\|_{V_h} \|\mathbf{w}_h\|_{V_h}}, \qquad \mathbf{u}_h, \mathbf{v}_h, \mathbf{w}_h \in V_h,$$

$$\mathbf{f}_h = \text{Proj}_{V_h} \mathbf{f}.$$

We shall need the hypothesis:

(H.1′) $$N_h R^2 \|\mathbf{f}_h\|_{V_h} \leqslant 1 - \delta, \qquad \delta > 0.$$

On $V \times W$ we shall need the following fundamental hypothesis (cf. Brezzi [3]). There exists $k > 0$, such that:

$$\sup_{\mathbf{u}_h \in V_h} \frac{(\text{div}_h \mathbf{u}_h, p_h)}{\|\mathbf{u}_h\|_{V_h}} \geqslant k \|p_h\|_{W_h}, \qquad \text{for all} \quad p_h \in W_h. \tag{8}$$

We can now state the following results.

THEOREM 1. *Under hypothesis* (H.1), *problem* $P$ (*resp.* $P_\epsilon$) *has a unique solution* $\{\mathbf{u}, p\}$ (*resp.* $\{\mathbf{u}_\epsilon, p_\epsilon\}$) *and*

$$\|\mathbf{u} - \mathbf{u}_\epsilon\|_V + \|p - p_\epsilon\|_W \leqslant C\epsilon. \tag{9}$$

THEOREM 2. *Under* (H.1), (H.1′), *and* (8), *let* $\{\mathbf{u}_{h,\epsilon}, p_{h,\epsilon}\}$ *be the unique solution of problem* $P_\epsilon$ *formulated on* $V_h \times W_h$, $\{\mathbf{u}, p\}$ *the unique solution of problem* $P$, *and* $\{\mathbf{u}_h, p_h\}$ *the unique solution of the corresponding problem on* $V_h \times \tilde{W}_h$ *then*:

$$\|\mathbf{u} - \mathbf{u}_{h,\epsilon}\|_{V_h} + \|p - p_{h,\epsilon}\|_{W_h} \leqslant C_1\epsilon + \|\mathbf{u} - \mathbf{u}_h\|_{V_h} + \|p - p_h\|_{W_h}. \tag{10}$$

For proof see [1].

*Note.* (a) Equation (10) shows that once one has chosen the proper approximation spaces $V_h$, $W_h$ for the original problem, the perturbed equations will provide a solution as close as one wishes to $(\mathbf{u}_h, p_h)$. Thus one can solve problem $P_\epsilon$ on

$V_h \times W_h$ without losing any significant accuracy compared to problem $P$, provided that $\epsilon$ is small enough.

(b) In problem $P_\epsilon$ the pressure automatically satisfies $\int_\Omega p_\epsilon = 0$, for the homogeneous boundary condition case.

## 3. A New Finite Element

The central point in Theorem 2 is (8): the proper definition of an operator $\mathrm{div}_h(\cdot)$. Following Fortin [8] and Crouzeix and Raviart [7] we extend their definition of $\mathrm{div}_h(\cdot)$ to a quadrilateral element. First note that in (6'a), (6'b) we can eliminate the pressure term $p_{h,\epsilon}$ to obtain instead of (6'a), (6'b):

$$\frac{1}{R}\, a(\mathbf{u}_{h,\epsilon}, \mathbf{v}_h) + b(\mathbf{u}_{h,\epsilon}, \mathbf{u}_h, \mathbf{v}_h) + \frac{1}{\epsilon}\,(\mathrm{div}_h\, \mathbf{u}_{h,\epsilon}, \mathrm{div}_h\, \mathbf{v}_h) = (\mathbf{f}_h, \mathbf{v}_h) \tag{11}$$

and what we have to construct is the matrix representation of

$$\frac{1}{\epsilon}\,(\mathrm{div}_h\, \mathbf{u}_{h,\epsilon}, \mathrm{div}_h\, \mathbf{v}_h).$$

Let $\hat{Q}$ be the unit reference quadrilateral (Fig. 1) in the reference plane. We consider the nine-node $Q_2$ finite element (where $Q_s$ is the space of polynomials of degree $s$

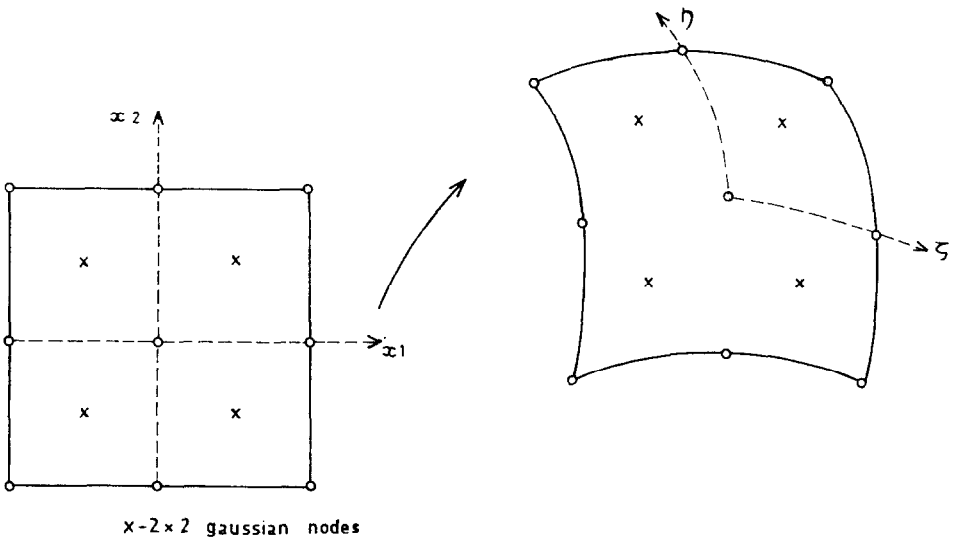


FIG. 1. Nine-node isoparametric element.

in each variable). The shape functions are given by standard Lagrangian interpolation,

$$l_i = \begin{cases} \frac{1}{4}\xi_i\eta_i\xi\eta(1 + \xi_i\xi)(1 + \eta_i\eta), & i = 1, 3, 5, 7, \\ \frac{1}{2}\eta_i\eta(1 + \eta_i\eta)(1 - \xi^2), & i = 2, 6, \\ \frac{1}{2}\xi_i\xi(1 + \xi_i\xi)(1 - \eta^2), & i = 4, 8, \\ (1 - \xi^2)(1 - \eta^2), & i = 9, \end{cases}$$

where $(\xi_i, \eta_i)$ are the nodal coordinates.

For the definition of $W_h$ (pressure term) we shall use $Q_1$. Note that $W_h \subset L^2(\Omega)$ so that we do not have interelement continuity for the pressure. In the following discussion, until Section 4, we drop the subscript $h$ from $\mathbf{u}_h$, for ease of notation.

Now we introduce:

$$\int_{\hat{Q}} \operatorname{div}_h \mathbf{u}\phi(x)\, dx = \int_{\hat{Q}} \operatorname{div} \mathbf{u}\phi(x)\, dx, \qquad \text{for all} \quad \phi \in Q_1. \tag{12}$$

This is nothing but the definition of the projection of div $\mathbf{u}$ on the space of bilinear polynomials over $Q_1$.

Let $\alpha_1, \alpha_2, \alpha_3, \alpha_4$ be the four points of the $2 \times 2$ quassian quadrature on $\hat{Q}$. We know that this set of points is $Q_1$ unisolvent (cf. Ciarlet and Raviart [6]), i.e., a basis of $Q_1$ is given by the four bilinear shape functions $\phi_1, \phi_2, \phi_3, \phi_4$ at nodes $\alpha_1, \alpha_2, \alpha_3, \alpha_4$. So that (12) is equivalent to the four equations:

$$\int_{\hat{Q}} \operatorname{div}_h \mathbf{u}\phi_i\, dx = \int_{\hat{Q}} \operatorname{div} \mathbf{u}\phi_i\, dx; \qquad i = 1, 2, 3, 4. \tag{12'}$$

The $2 \times 2$ gaussian quadrature rule is exact for all polynomials in $Q_3$. Now if $\mathbf{u} \in Q_2$, div $\mathbf{u} \cdot \phi_i \in Q_3$ so that

$$\int_{\hat{Q}} \operatorname{div} \mathbf{u}\phi_i\, dx$$

is exactly computed by the $2 \times 2$ rule! By definition of $\phi_i$ and (12') we obtain four identities:

$$\operatorname{div}_h \mathbf{u}(\alpha_i) = \operatorname{div} \mathbf{u}(\alpha_i); \qquad i = 1, 2, 3, 4. \tag{13}$$

As $\operatorname{div}_h(\cdot)$ is in $Q_1$, we have on $\hat{Q}$

$$\operatorname{div}_h \mathbf{u} = \sum_1^4 \operatorname{div} \mathbf{u}(\alpha_i) \cdot \phi_i(x). \tag{14}$$

Let $\mathbf{q}$ be the standard vector of all 18 nodal values of $\mathbf{u}$ on $Q$:

$$\mathbf{q}^T = (u_1(1), u_2(1), u_1(2), \ldots, u_1(9), u_2(9)).$$

According to (11) we have to compute the matrix $K_1$ such that:

$$\int_{\hat{Q}} \operatorname{div}_h{}^2 \mathbf{u}\, dx = \mathbf{q}^T K_1 \mathbf{q}. \tag{15}$$

Let $w_i$ ($i = 1, 2, 3, 4$), be the weights of the $2 \times 2$ guassian quadrature, then in (15) we have by (14):

$$\int_{\hat{Q}} \operatorname{div}_h^2 \mathbf{u}\, dx = \sum_{i=1}^{4} w_i \operatorname{div}_h^2 \mathbf{u}(\alpha_i). \tag{16}$$

We see that $K_1$ can be obtained by computing $\int_{\hat{Q}} \operatorname{div}^2 \mathbf{u}\, dx$ with the $2 \times 2$ guassian quadrature rule.

This rule is of course inexact for $\operatorname{div}^2 \mathbf{u}$, but by using reduced integration we directly obtain the stiffness matrix corresponding to our operator $\operatorname{div}_h(\cdot)$!

In the case of a "triangulation" made up of rectangles whose sides are parallel to the $Ox_1$, $Ox_2$ axis we can obtain error estimates in $O(h^2)$. The more general isoparametric element is a difficult case, due to the presence of a nonconstant Jacobian. Numerical examples as well as an error analysis of this element are currently under study.

## 4. Application to Navier–Stokes Equations

In all that follows $V_h$ is taken to be the finite-dimensional space defined by a given FEM "triangulation."

The stationary approximate problem is to find $\mathbf{u}_h$ such that

$$\frac{1}{R} a(\mathbf{u}_h, \mathbf{v}_h) + \hat{b}(\mathbf{u}_{h,\epsilon}, \mathbf{u}_{h,\epsilon}, \mathbf{v}_h) + \frac{1}{\epsilon}(\operatorname{div}_h \mathbf{u}_{h,\epsilon}, \operatorname{div} \mathbf{v}_h) = (\mathbf{f}_h, \mathbf{v}_h) \tag{17}$$

for all $\mathbf{v}_h \in V_h$.

Problem (17) is nonlinear. To solve it we shall use the following algorithm:

Omitting indices $h$ and $\epsilon$, let $\mathbf{u}^0$ be an initial guess (for instance, $\mathbf{u}^0 = 0$), let $\mathbf{u}^n$ be the $n$th iterate, compute $\mathbf{u}^{n+1}$ solution of

$$\frac{1}{R} a(\mathbf{u}^{n+1}, \mathbf{v}_h) + \hat{b}(\mathbf{u}^n, \mathbf{u}^{n+1}, \mathbf{v}_h) + \frac{1}{\epsilon}(\operatorname{div}_h \mathbf{u}^{n+1}, \operatorname{div}_h \mathbf{v}_h) = (\mathbf{f}_n, \mathbf{v}_n). \tag{18}$$

Derivation of the stiffness matrices $A$, $B(\mathbf{u})$ for $a(\mathbf{u}^{n+1}, \mathbf{v}_h)$ and $\hat{b}(\mathbf{u}^n, \mathbf{u}^{n+1}, \mathbf{v}_h)$ is carried out by $3 \times 3$ gaussian quadrature. $A$ is a symmetric positive definite matrix and $B(u)$, by the definition of the functional $\hat{b}(\mathbf{u}, \mathbf{v}, \mathbf{w})$ is an antisymmetric matrix for all $\mathbf{u}$. $K_1$, the stiffness matrix for the penalty term $(\operatorname{div}_h \mathbf{u}^{n+1}, \operatorname{div}_h \mathbf{v}_h)$, is also symmetric and nonnegative definite; thus the total stiffness matrix of (18), $A + (1/\epsilon) K_1 + B(u)$ is positive definite: This is easily shown as follows.

Let $X$ be any vector; then

$$X^T \left(A + \frac{1}{\epsilon} K_1 + B(u)\right) X = X^T \left(A + \frac{1}{\epsilon} K_1\right) X + X^T B(u) X.$$

Now $X^T B X = -X^T B^T X = -(X^T B X)^T$, since $B^T = -B \Rightarrow X^T B X = 0$. Since $X^T(A + (1/\epsilon) K_1) X > 0$ we have

$$X^T \left( A + \frac{1}{\epsilon} K_1 + B(u) \right) X > 0.$$

The convergence test will be on $| \mathbf{u}^{n+1} - \mathbf{u}^n |$. Now (18) is a linear problem, whose matrix depends on $n$th iterate $\mathbf{u}^n$ through $\hat{b}(\mathbf{u}^n, \mathbf{u}^{n+1}, \mathbf{v}_h)$. It can be shown (cf. [1]) that this algorithm is convergent under the same hypotheses as those of Theorem 2. Convergence is usually fast, although use of the Newton–Raphson method would probably result in more rapid convergence at higher Reynold's number [12]. The pressure field is recovered from the velocity field by $p = (1/\epsilon) \operatorname{div}_h \mathbf{u}_h |_{2\times 2}$ Gaussian points.

After assembly at the element level, the degrees of freedom related to the midpoint node are condensed (i.e., eliminated), thus reducing the size and bandwidth of the final system.

For the time dependent problem we use a fully implicit scheme. Again dropping $h$ and $\epsilon$, let $\mathbf{u}^k$ the solution at time $k \cdot dt$. We solve for time $(k + 1) \cdot dt$:

$$\left( \frac{\mathbf{u}^{k+1} - \mathbf{u}^k}{\Delta t}, \mathbf{v}_h \right) + \frac{1}{R} a(\mathbf{u}^{k+1}, \mathbf{v}_h) + \hat{b}(\mathbf{u}^{k+1}, \mathbf{u}^{k+1}, \mathbf{v}_h) + \frac{1}{\epsilon} (\operatorname{div}_h \mathbf{u}^{k+1}, \operatorname{div}_h \mathbf{v}_h)$$
$$= (\mathbf{f}_h^{k+1}, \mathbf{v}_h). \tag{19}$$

The nonlinear equation (19) is solved by (18). The initial guess being $\mathbf{u}^k$, the algorithm converges in a small number of iterations.

## 5. Influence of the Value of $\epsilon$

To examine the effect of the penalization parameter $\epsilon$ on the computed velocity field, two analytical examples were studied using both the nine-node element as previously described and the eight-node isoparametric element as used by Zienkiewicz and Godbole [21].

The analytical examples were: compute the $(u, p)$ solution on the unit square $\Omega$ of

$$-\Delta \mathbf{u} + \operatorname{grad} p = \mathbf{F} \qquad \text{on } \Omega,$$
$$\mathbf{u} |_{\partial\Omega} = 0,$$

for

(1) $\mathbf{F}_1$: $F_{x_1} = 128[x^2(x-1)^2 12(2y-1) + 2(y-1)(2y-1)\, y(12x^2 - 12x + 2)]$,
$F_{y_1} = F_{x_1}(y, x)$;

(2) $\mathbf{F}_2$: $F_{x_2} = F_{x_1} + y - \frac{1}{2}$,
$F_{y_2} = F_{x_2}(y, x)$.

The solution of (1) is:

$$\mathbf{u}: u_{x_1} = -256x^2(x-1)^2\, y(y-1)(2y-1), \qquad p = 0,$$
$$u_{y_1} = -u_{x_1}(y, x),$$

and the solution of (2) is $\mathbf{u}$ as problem (1) and $P = (x - \frac{1}{2})(y - \frac{1}{2})$. The element mesh chosen was a regular $10 \times 10$ mesh of square elements. The relative error in the velocity field was calculated for values of $\epsilon = 10^{-1}$ through $10^{-9}$ by:

$$\text{rel. error } \mathbf{u} = \left( \sum_{\text{nodes}} \frac{\sum_i \| \mathbf{u}_e - \mathbf{u}_c \|^2}{\sum_i \| \mathbf{u}_e \|^2} \right)^{1/2}$$

where

$\mathbf{u}_c$ = computed solution,

$\mathbf{u}_e$ = exact solution.

The relative errors are tabulated in Table I.

TABLE I

Effect of Penalization Parameter

| | Example 1 | | Example 2 | |
|---|---|---|---|---|
| | 8 pt. elt. | 9 pt. elt. | 8 pt. elt. | 9 pt. elt. |
| $10^{-1}$ | 0.0015916 | 0.0014885 | 0.0006165 | 0.0000920 |
| $10^{-2}$ | 0.0011780 | 0.0002186 | 0.0011624 | 0.0000977 |
| $10^{-3}$ | 0.0033015 | 0.0001004 | 0.0033011 | 0.0000983 |
| $10^{-4}$ | 0.0062272 | 0.0000984 | 0.0062272 | 0.0000984 |
| $10^{-5}$ | 0.0071120 | 0.0000984 | 0.0071120 | 0.0000984 |
| $10^{-7}$ | 0.0072296 | 0.0000988 | 0.0072296 | 0.0000988 |
| $10^{-h}$ | 0.0072156 | 0.0001028 | 0.0072156 | 0.0001028 |

The dramatic improvement of the nine-node element over the eight-node element is immediately evident from these results. Similar behavior has been observed by Malkus [15].

For the nine-node element, the effect of decreasing the value of $\epsilon$ is seen to stabilize from $\epsilon = 10^{-3}$, one order less than the value of $h^2 = 10^{-2}$. This is as predicted by Theorem 2. The small increase in the relative error of $\mathbf{u}$, starting from $10^{-7}$ can be attributed to the beginning of the effects of round-off error.

For the eight-none element the effect of the penalization for decreasing values of $\epsilon$ steadily worsens from $10^{-2}$ although the behavior is better than might be expected of such a penalization method.

The above results and the authors' experience indicate that a value of $\epsilon = 10^{-2}h^2$ is sufficient for all computational purposes.

## 6. Numerical Examples

All the numerical examples presented in this paper were run on the CDC Cyber 74 at the Computation Centre of the Hebrew University of Jerusalem. The program was developed by the second author with much valuable assistance of Yitzhak Hasbani of the Computation Centre; it was written in Fortran and compiled by the CDC FTN compiler using its optimizer.

The system of equations $A(\mathbf{u})\,\mathbf{u} = B$ resulting from the FEM analysis was solved by the iterative method $A(\mathbf{u}_n)\,\mathbf{u}_{n+1} = B$. At each iteration this system of linear equations was solved using an LU decomposition algorithm without pivoting.

A "skyline" storage mode was adopted for the matrix A, however, even using this storage mode, the memory available made an in-core solution impossible, so an out-of-core solution algorithm, "skyline LU decomposition by blocks," was developed and coded by Hasbani [11]. All the velocity vector and pressure contour plots presented are the original and unretouched computer plots of the numerical results. All plots were done on a Gerber flat-bed incremental plotter.

### 6.1. *Wall-Driven Cavity*

The classical problem of a wall-driven cavity on a unit square, $\mathbf{u} = 1$ along the entire upper boundary including the corner nodes (cf. Fig. 2), was chosen in order to investigate the convergence and stability properties of the previously described finite element technique. The modelization used was a simple "triangularization"

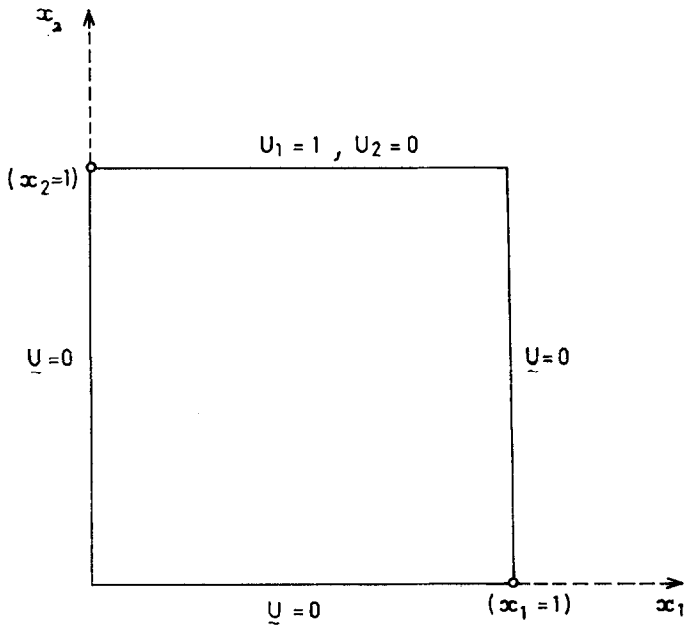


FIG. 2. Wall driven cavity.

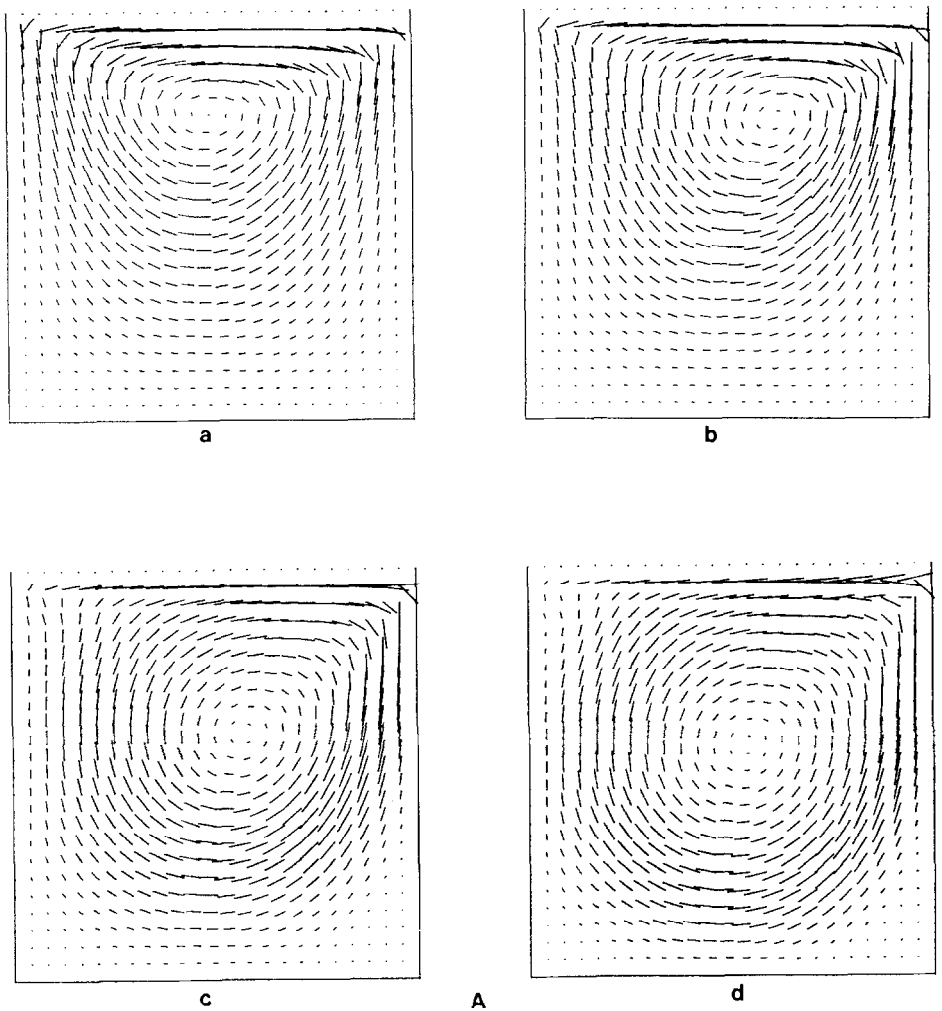


FIG. 3A. Velocity vector plots for square cavity. Reynolds number equal to 0(a); 100 (b); 400 (c); 1000 (d).

into $N^2$ equal squares. It might be objected that this does not take full advantage of the FEM but such a grid is useful for the study of convergence in terms of $h = 1/N$ as well as for underlining the problems that might occur when the actual solution is not smooth enough.

Computations were carried out on four different grids; $5 \times 5$, $7 \times 7$, $10 \times 10$, and $12 \times 12$, for Reynolds numbers of Re = 0(0.001), 100, 400, 1000. The velocity vector field plots for the $12 \times 12$ discretization are shown in Figs. 3A, and 3B gives the pressure contour plots for the same four cases. Looking at the uppermost nodes in the four diagrams of Fig. 3A it can be seen that with increasing Reynolds number

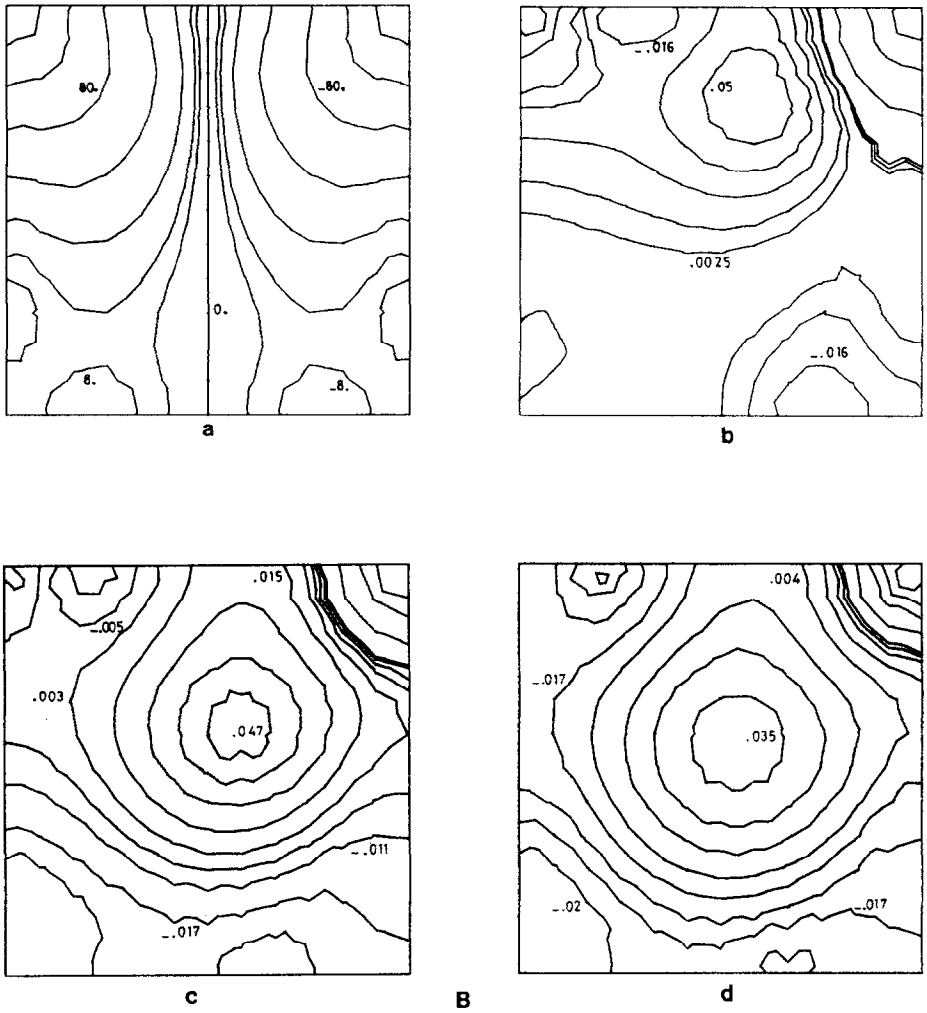


FIG. 3B. Pressure contour plots for square cavity. Reynolds number equal to 0 (a); 100 (b); 400 (c); 1000 (d).

there is an increasing oscillation in the right-hand corner. This is clearly due to the singularity in the velocity field at the corner. In the $5 \times 5$ grid at $\mathrm{Re} = 1000$ this oscillation is very marked, to the extent that a large part of the velocity field is distorted. This effect rapidly diminished with mesh refinement.

The profiles of the horizontal velocity along the center line of the cavity ($x = 0.5$) for each of the velocity fields of Fig. 3A are compared in Fig. 4A. These profiles show almost exact agreement with those of Burgraff [4]. It is also evident the profile for $\mathrm{Re} = 1000$ is indeed approaching the theoretical profile for $\mathrm{Re} = \infty$. The presence of a thin boundary layer at high Reynolds number is evidenced by the

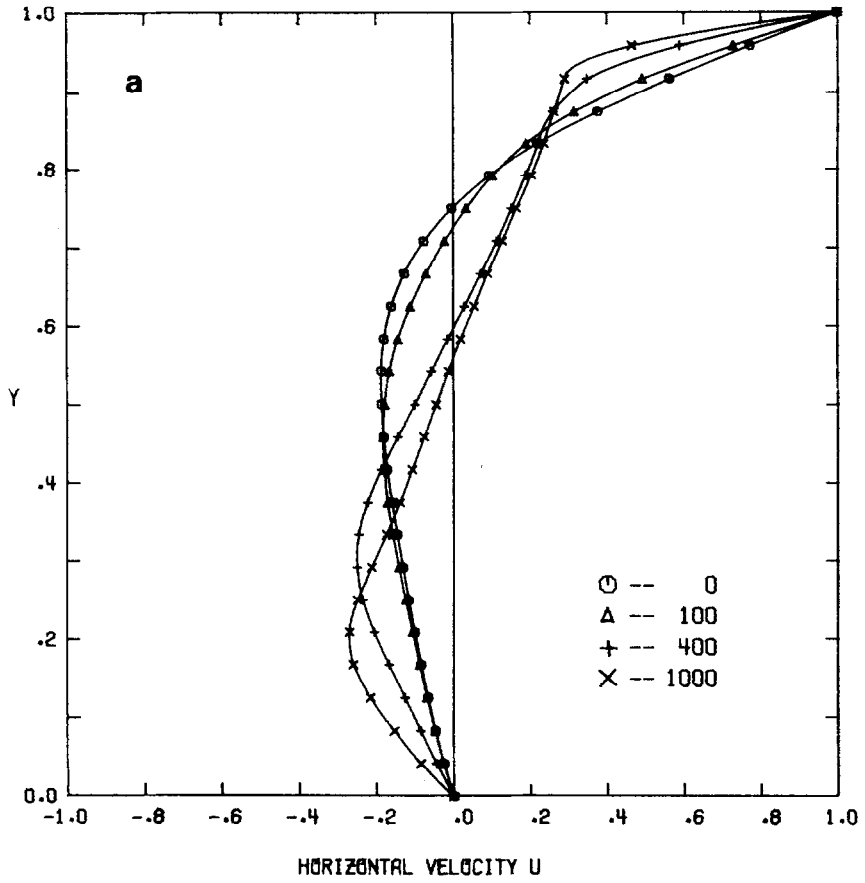


FIG. 4a. Velocity profile for 12 × 12 grid.

Re = 1000 profile. This layer is seen to be much thicker at Re = 400 and is not present at all at Re = 100. Figure 4b compares similar velocity profiles to those of Fig. 4a, this time for the four different sized grids at the Reynolds number 400. Once again the convergent effect of mesh refinement is clear and it can be seen that further refinement of the mesh above 10 × 10 does not result in any significant change in the velocity profile.

The center point ($\mathbf{u} = 0$) of the main eddy in the cavity was computed for the four Reynolds numbers at each of the various grid sizes (cf. Table II). Also recorded in this table are the same results as measured from the graphs presented by Burgraff. The convergent effect of mesh refinement is again seen in this table. The movement of the eddy center downwards, first in the direction of the boundary flow and then toward the center of the cavity, is evident.

At higher Reynolds numbers it is known that counter-eddies appear in the two bottom corners of the cavity. Figure 5 is a "blow-up" of the two bottom corners for

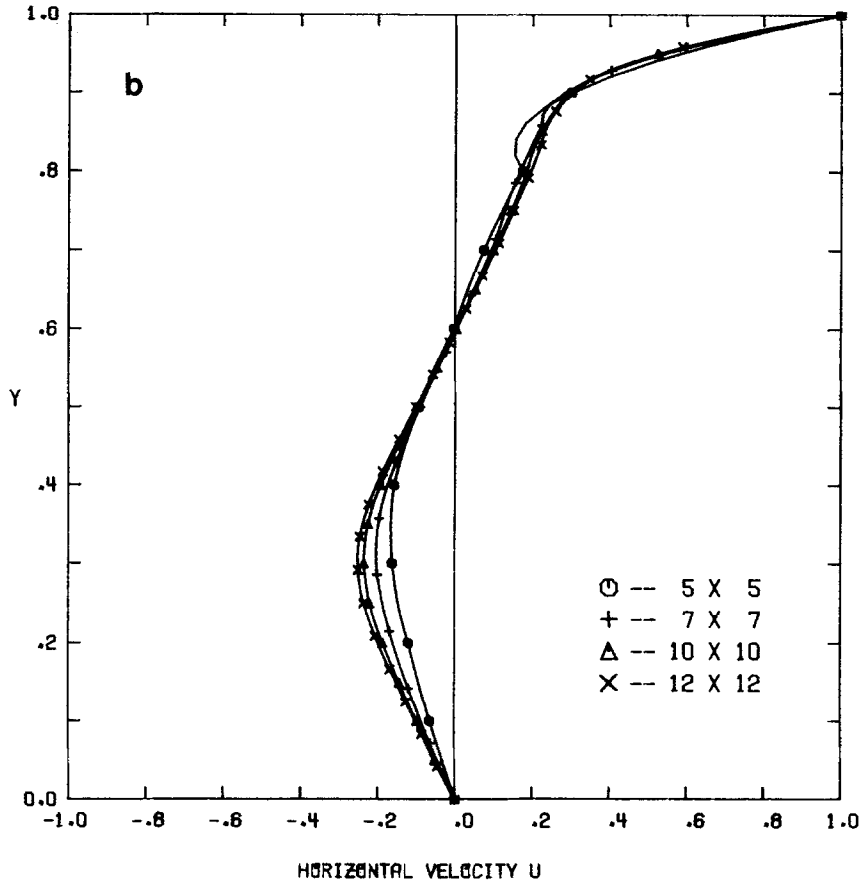


FIG. 4b. Velocity profiles for Re = 400.

TABLE II

Center Point (u = 0) of Main Eddy

| Grid size | Reynolds No. | | | |
|---|---|---|---|---|
| | 0 | 100 | 400 | 1000 |
| 5 × 5 | (0.50, 0.72) | (0.62, 0.72) | (0.61, 0.62) | (0.59, 0.57) |
| 7 × 7 | (0.50, 0.73) | (0.62, 0.73) | (0.59, 0.61) | (0.56, 0.56) |
| 10 × 10 | (0.50, 0.74) | (0.62, 0.73) | (0.58, 0.61) | (0.55, 0.56) |
| 12 × 12 | (0.50, 0.74) | (0.62, 0.73) | (0.57, 0.61) | (0.54, 0.56) |
| Burgraff | (0.50, 0.76) | (0.62, 0.74) | (0.56, 0.61) | — |

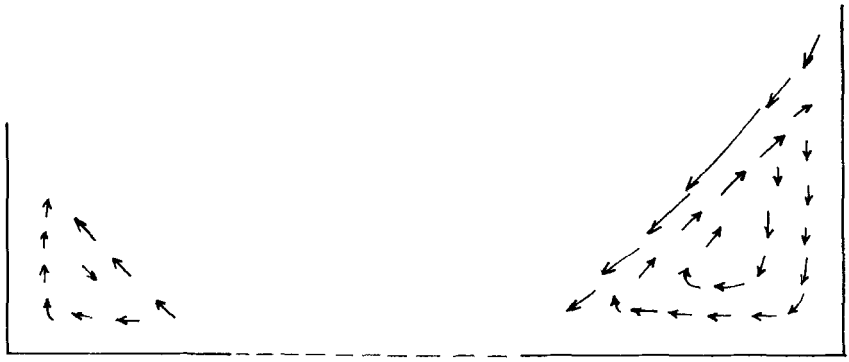

FIG. 5. "Blow-up" of corner eddies.

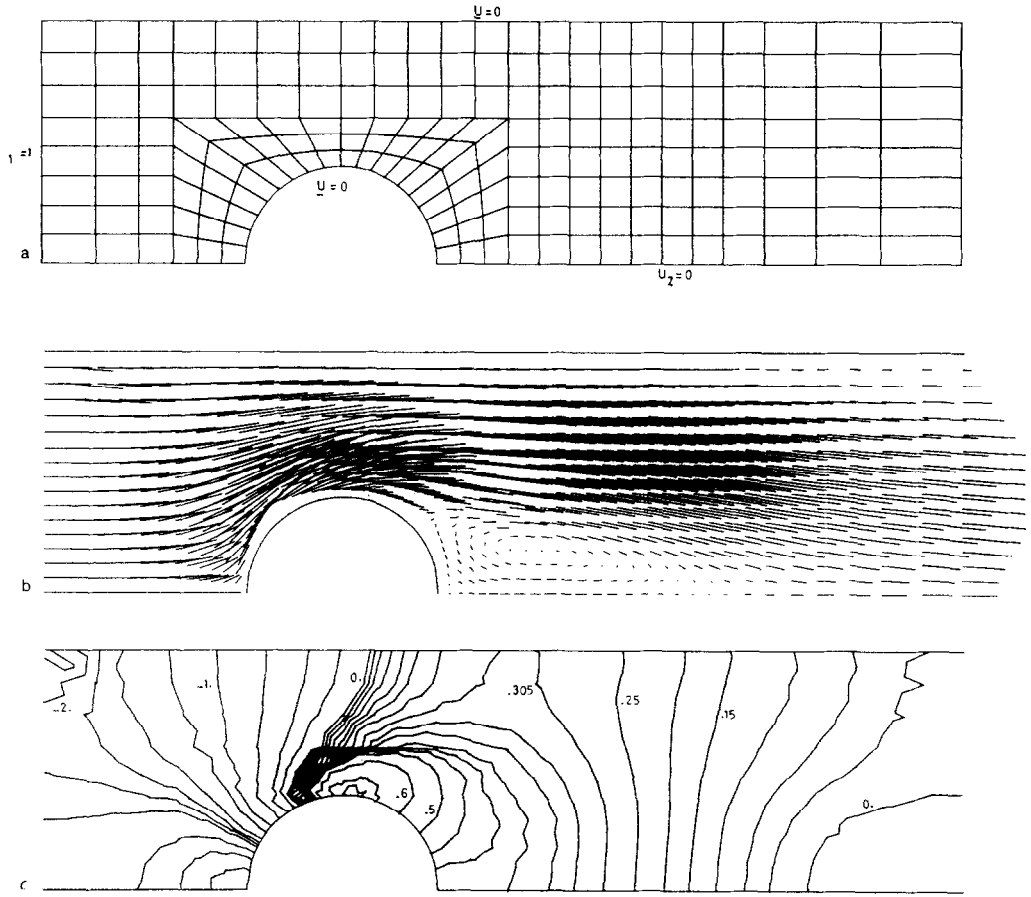


FIG. 6. Flow past a circular cylinder. (a) Computational grid + boundary conditions. (b) Velocity vector plot. (c) Pressure contour plot.

Re = 1000, 12 × 12 grid. The two counter-eddies are clearly visible. In the case of the 12 × 12 grid, with a convergence parameter of $10^{-4}$, the Reynolds number 100 converged in 8 iterations, Re = 400 in 12 and Re = 1000 in 22 iterations; the execution time of each iteration being 5.5 CP seconds. The initial iterative guess in all cases was $\mathbf{u}_0 = \mathbf{0}$ within the cavity and $\mathbf{u}_0 = 1$ in the $x$ direction along the entire upper boundary. Tests were made using the next lower Reynold's number as the initial guess and it was found that this caused a reduction in the number of iterations by a maximum of two iterations only. This is a distinguishing feature of the quasi-linearization iterative method as against the Newton–Raphson method [12].

In all these examples the value of the penalization parameter, $\epsilon$, was $10^{-5}$. In order to test that a value of $\epsilon = 10^{-2}h^2$ is sufficient for computational purposes the 12 × 12,

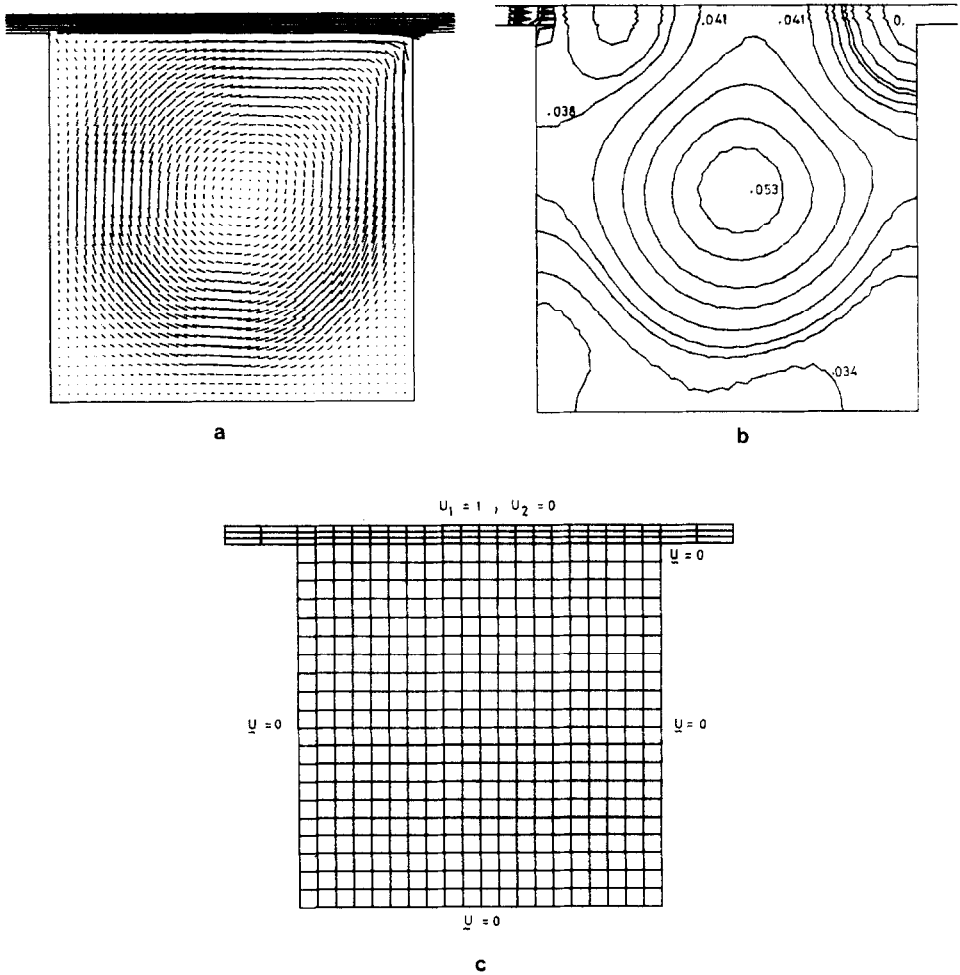


FIG. 7. High Reynolds number flow. (a) Velocity vector plot. (b) Pressure contour plot. (c) Computational grid.

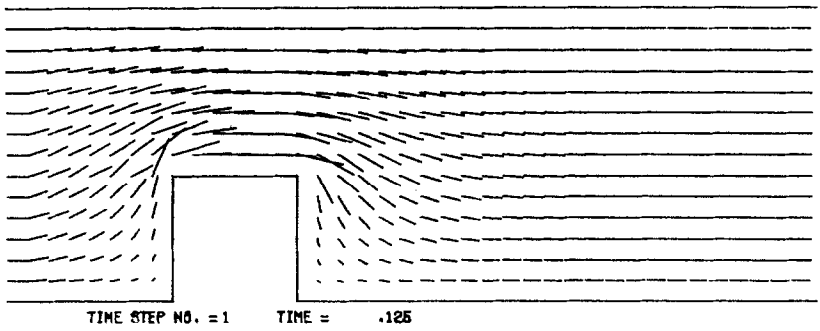


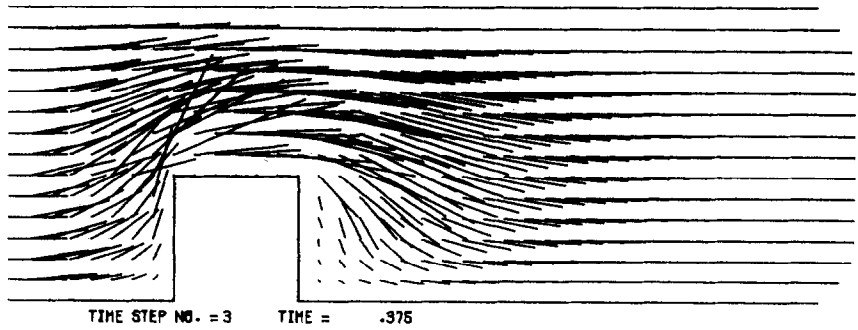


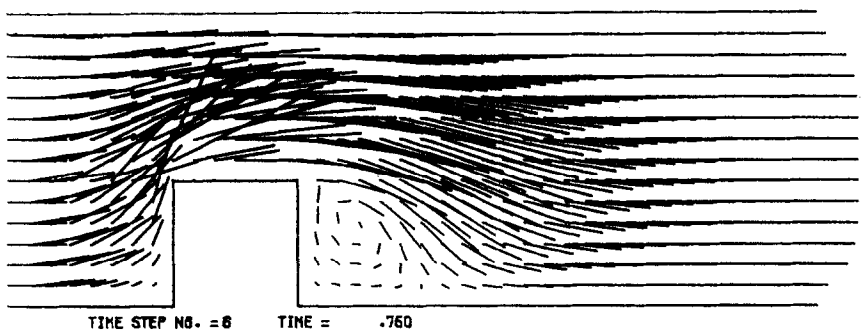


Re = 400 problem was recomputed using a value of $\epsilon = 10^{-3}$. It was found that both the pressure and velocity field for $\epsilon = 10^{-5}$ and $\epsilon = 10^{-3}$ differed only in the fifth significant digit. To illustrate the stability and capabilities of the method at higher Reynolds numbers, the cavity problem was computed for a Reynolds number of 2000. In order to eliminate the singularities in the velocity field at the two top corners the

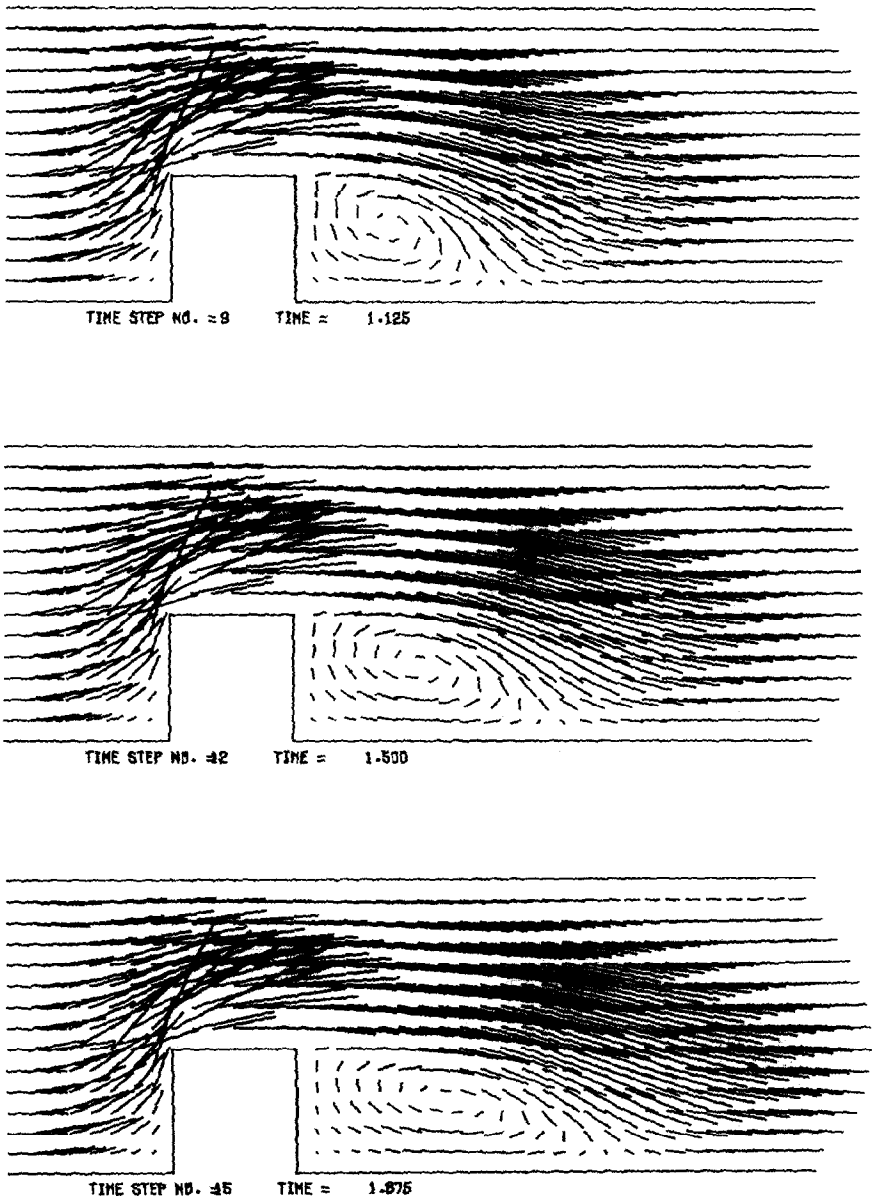


FIG. 8. Time dependent flow past a step.

flow was driven by a thin channel (cf. Fig. 7a)) rather than by an imposed velocity on the top boundary of the cavity. The computed velocity vector field and pressure contour plots are shown in Figs. 7b and c, respectively. It is clear, on comparison with the result for $Re = 1000$, that the center of the main eddy has moved closer to the center of the cavity. It is also evident that the flow is settling into a symmetric

form, with a slow central symmetric "square" eddy and a thin faster boundary layer flow. This is as expected for a highly viscous flow in a square cavity.

The solution converged (criterion $10^{-4}$) in 20 iterations, each iteration taking 37 seconds CP time.

### 6.2. *Flow Past a Circular Cylinder*

To illustrate the versatility of the FEM (in this particular example, the ease of treatment of curved boundaries), the flow past a circular cylinder in an infinite channel was computed. Since the steady state problem was considered by the symmetry property of the solution, only the top half of the domain was modeled. The various boundary conditions and computational grid used are shown in Fig. 6a. The outflow boundary condition used was that which arises "naturally" from (6′).

The mesh was generated automatically by the software QMESH, developed by Jones [13]. The Reynolds number used was 75 and the penalization parameter $\epsilon$ was $10^{-5}$. The solution converged in 14 iterations, the convergence criterion being $10^{-4}$, each iteration taking 7.8 CP seconds.

The resulting velocity vector field and pressure contours are shown in Figs. 6b and c. These results are in agreement with various experimental results.

### 6.3. *Time-Dependent Flow*

As the subject of time-dependent flows and the question of which algorithm to use to solve the resulting set of equations

$$M\frac{d\mathbf{u}}{dt} + K(\mathbf{u})\mathbf{u} = \mathbf{F}, \qquad M, K = n \times n \text{ matrices}, \; n = \text{no. of degrees of freedom}$$

is a very wide, diverse one and will be the subject of a separate paper, we present here without comment the time-dependent flow of a fluid past a square step (cf. Fig. 8). The algorithm used was the fully implicit scheme described by Eq. (19). Steady state flow was reached after 21 time steps of $dt = 0.125$ seconds.

## Conclusion

The finite element construction discussed in this paper has two interesting properties. First it is of a high order of accuracy, allowing the treatment of large Reynolds number problems without any special treatment of the nonlinear term of the Navier–Stokes equations. Thus in the cavity problem, Re = 1000, a step size of $h = 1/12$ (a total of 625 nodal points) is sufficient.

Second, the judicious use of the penalty function with reduced integration allows us to eliminate the pressure unknown altogether, and so the introduction of unnecessary unknowns is avoided. This penalization method results in a stable positive definite system, thus enabling solution by a Gaussian elimination algorithm without pivoting.

Further developments currently under study are time-dependent algorithms, the extension of the theory to three dimensions, and the adaptation of the method to very high Reynolds numbers.

## ACKNOWLEDGMENT

The authors wish to thank the reviewers for their comments and suggestions, which were found to be most helpful.

## REFERENCES

1. M. BERCOVIER, These de Doctorat d'État, Rouen, 1976.
2. M. BERCOVIER AND E. LIVNE, A 4-CST quadrilateral element for incompressible and nearly incompressible materials, *Calcolo*, to appear.
3. F. BREZZI, On the existence, uniqueness and approximation of saddle point problems arising from Lagrange multipliers, RAIRO, R. 2 Aout (1974).
4. O. D. BURGRAFF, Analytical and numerical studies of the structure of steady separated flows, *J. Fluid Mech.* **24** (1966).
5. A. J. CHORIN, A numerical method for solving incompressible viscous problems, *J. Computational Phys.* **2** (1967).
6. P. G. CIARLET AND P. A. RAVIART, The combined effect of curved boundaries and numerical integration in isoparametric finite element methods, *in* "The Mathematical Foundations of the F.E.M. with Applications to P. D. E." (A. K. Aziz, Ed.), Academic Press, New York, 1972.
7. M. CROUZEIX AND P. A. RAVIART, Conforming and non-conforming elements methods for solving the stationary Stokes equations, RAIRO, R.3 (1973).
8. M. FORTIN, These de Doctorat d'État, Paris, 1972.
9. R. S. FALK, On analysis of the penalty and extrapolation method for the stationary Stokes equations, *in* "Advances in Computer Methods for P.D.E.,'s" (R. Vichnevetsky Ed.), Proceedings of AICA Symposium, 1975.
10. I. Fried, Finite element analysis of incompressible for incompressible viscous flows, *Internat. J. Solids Structures* **10** (1974), 993–1002.
11. Y. HASBANI AND M. ENGELMAN, Out-of-core solution algorithms for non-symmetric sparse matrices, *Computers and Fluids*, to appear.
12. T. J. R. HUGHES, R. L. TAYLOR, AND J. F. LEVY, "A Finite Element Method for Incompressible Viscous Flows," preprints of 2nd Int. Symp. on F.E.M. Methods in Flow Problems, S. Margherita Ligure, Italy, June 14–18, 1976.
13. R. JONES, "QMESH: A Self-Organising Mesh Generation Program," Technical Report SLA-73-1088, Sandia Laboratories, Alberquerque, N.M.
14. D. S. MALKUS, "Finite Element Analysis of Incompressible Solids," Ph.D. Thesis, Boston University, Boston, 1975.
15. D. S. MALKUS, Finite element displacement model valid for any value of the compressibility, *Internat. J. Solids Structures* **12** (1976), 731–738.
16. D. J. NAYLOR, Stresses in nearly incompressible materials by finite elements, *I.J.N.M.E.* **8** (1974).
17. M. C. PELISSIER, Resolution numerique de quelques problèmes raides en mécanique des milieux faiblement compressibles, *Calcolo*, to appear.
18. C. TAYLOR AND P. HOOD, A numerical solution of the Navier–Stokes equations using F.E.M. technique, *Computers and Fluids* **1** (1973).
19. R. TEMAN, Une méthode d'approximation de la solution des équations de Navier–Stokes, *Bull. Soc. Math. France* **96** (1968).

20. R. TEMAN, "*Navier–Stokes Equations*," North–Holland, Amsterdam, 1976.
21. O. C. ZIENKIEWICZ AND P. N. GODBOLE, Viscous incompressible flows with special reference to non-newtonian (plastic) fluids, *in* "Finite Element Method in Flow Problems," Wiley, New York, 1975.
22. O. C. ZIENKIEWICZ, C. R. TAYLOR, AND J. M. TOO, Reduced integration technique in general analysis of plates and shells, *I.J.N.M.E.* **3** (1971).